

Supporting Information

A Multi-Faceted Study of the Interactions Between CPO-27-Ni and Polyurethane and Their Impact on Nitric Oxide Release Performance

Simon M. Vornholt,^a Morven J. Duncan,^a Stewart J. Warrender,^a Rocio Semino,^b Naseem A. Ramsahye,^b Guillaume Maurin,^b Martin W. Smith,^c Jin-Chong Tan,^d David N. Miller,^a and Russell E. Morris^{*a,e}

a School of Chemistry, University of St Andrews, Purdie Building, St Andrews, KY16 9ST, UK

b ICGM, Univ. Montpellier, CNRS, ENSCM, Montpellier, France

c Defence Science and Technology Laboratory (Dstl), Porton Down, Salisbury, Wiltshire, SP4 0JQ, UK

d Department of Engineering Science, University of Oxford, Parks Road, Oxford OX1 3PJ, UK

e Department of Physical and Macromolecular Chemistry, Faculty of Sciences, Charles University Hlavova 8, 128 43 Prague 2, Czech Republic

**Corresponding author email: rem1@st-andrews.ac.uk*

Table of Contents:

I. List of Chemicals	2
II. Physical Characterization of MOF Powders.....	2
III. Particle Size Distribution of MOF Dispersions.....	3
IV. Characterisation of MOF Composite Films.....	5
V. NO Release Performance of MOF Powders and Composite Films.....	7
VI. Water Adsorption Isotherm Data.....	8
VII. Antibacterial Testing.....	9
VIII. Computational Methods	9
IX. References	14

I. List of Chemicals

Table S1. Chemicals used for synthesis of **CPO-27-Ni** (HT and RT) powders and composite materials.

Chemical	CAS Number	Vendor
Nickel acetate tetrahydrate	6018-89-9	Sigma-Aldrich
2,5-dihydroxyterephthalic acid	610-92-4	Dragon Chemicals
Polyurethane	68084-39-9	Sigma-Aldrich
Tetrahydrofuran	109-99-9	Fisher

II. Physical Characterization of MOF Powders

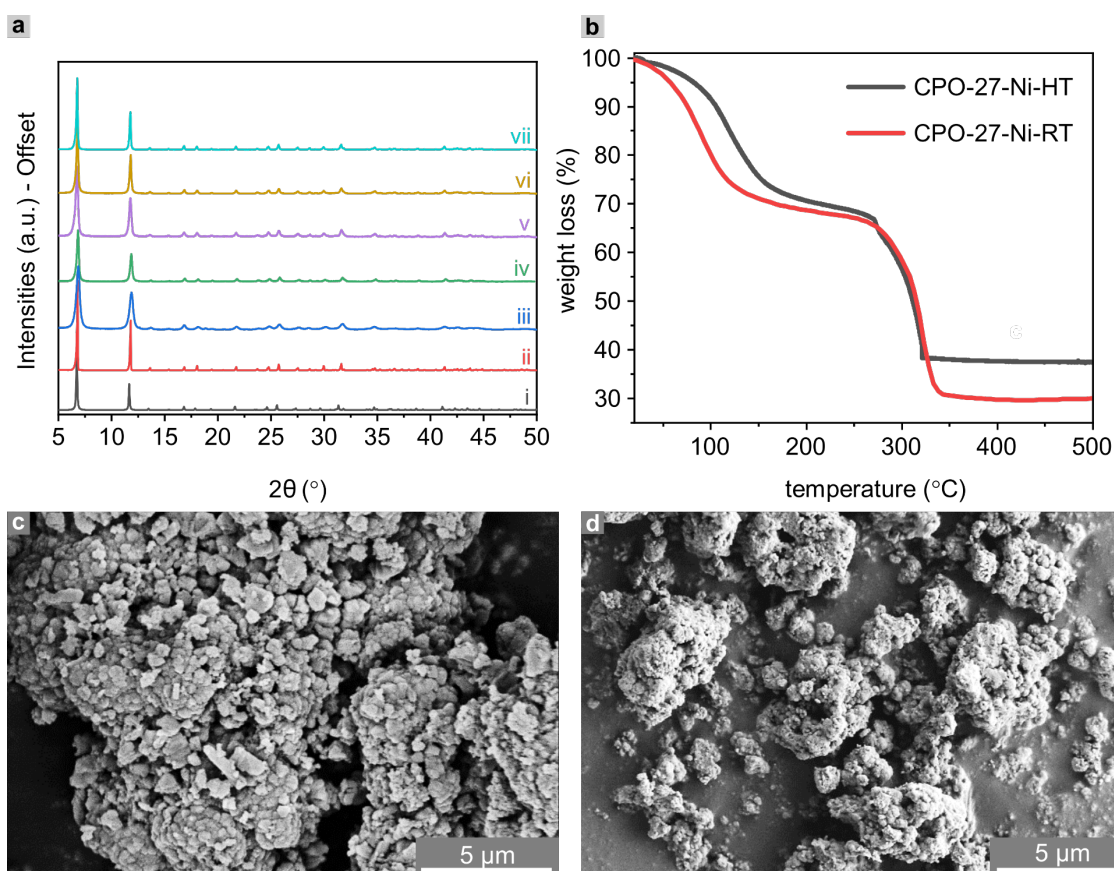


Figure S1. Characterization of powder **CPO-27-Ni-HT** and **CPO-27-Ni-RT** materials. a) PXRD patterns of **CPO-27-Ni** simulated pattern (i-gray), **CPO-27-Ni-HT** (ii-red), **CPO-27-Ni-RT** (iii-blue), **CPO-27-Ni-RT** after being mechanically dispersed and stored in water for 12 h (iv-green), and 6 months (v-purple), **CPO-27-Ni-RT** after being mechanically dispersed and stored in THF for 12h (vi-mustard) and 6 months (vii-cyan). b) Thermogravimetric analysis traces of **CPO-27-Ni-HT** (gray) and **CPO-27-Ni-RT** (red). SEM micrographs of c) **CPO-27-Ni-HT** and d) **CPO-27-Ni-RT**.

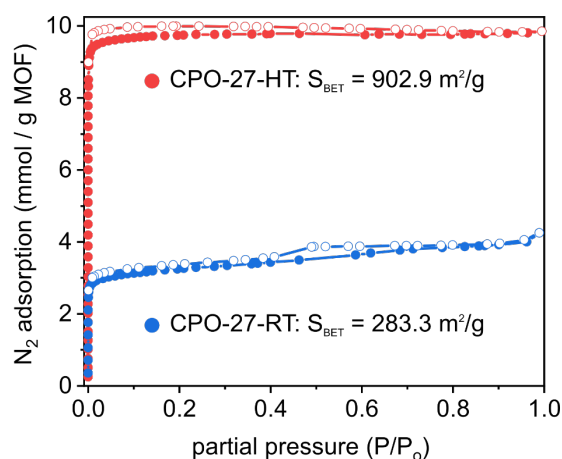


Figure S2. BET- N_2 isotherm plots for powder **CPO-27-Ni-HT** (red) and **CPO-27-Ni-RT** (blue) materials. Closed symbols refer to adsorption and open symbols to desorption.

III. Particle Size Distribution of MOF Dispersions

Table S2. Particle size measurements for powder **CPO-27-Ni-HT** and **CPO-27-Ni-RT** materials. Shown are values for as synthesized and mechanically dispersed materials with and without sonication. Data is averaged over 3 measurements.

MOF powder	Preparation	Particle Size		
		d (0.1) - μm	d (0.5) - μm	d (0.9) - μm
CPO-27-Ni-HT	as synthesized	1.44	13.10	41.5
CPO-27-Ni-HT	as synthesized, sonicated	0.96	10.16	28.40
CPO-27-Ni-HT	dispersed	0.11	1.04	4.07
CPO-27-Ni-HT	dispersed, sonicated	0.09	0.21	1.63
CPO-27-Ni-RT	as synthesized	0.69	9.45	129.05
CPO-27-Ni-RT	as synthesized, sonicated	0.58	4.25	89.54
CPO-27-Ni-RT	dispersed	1.32	2.33	4.01
CPO-27-Ni-RT	dispersed, sonicated	0.18	0.34	2.43

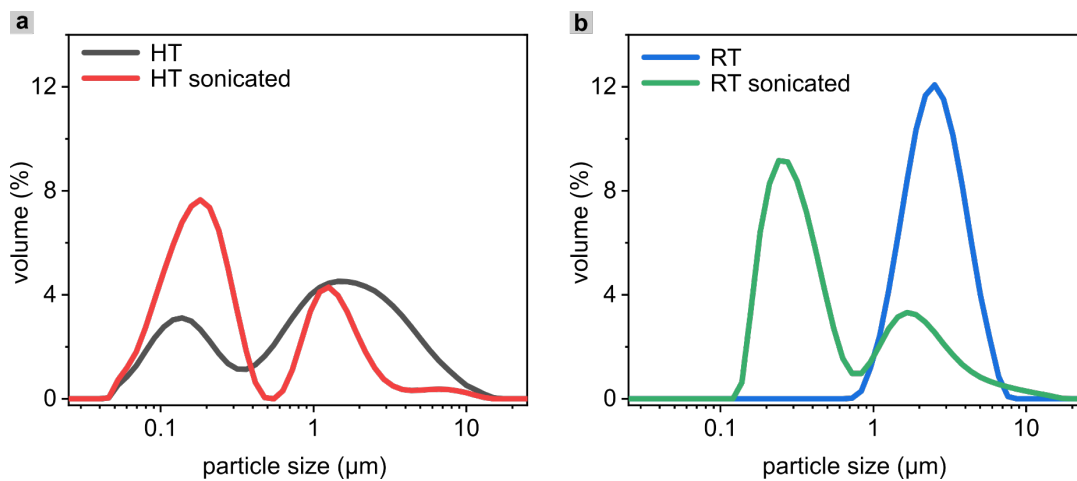


Figure S3. Particle size distribution of the MOF slurries after mechanical dispersion in THF. a) **CPO-27-Ni-HT** (gray – under stirring; red – after 3 min sonication) and b) **CPO-27-Ni-RT** (blue – under stirring; green – after 3 min sonication), aliquots of the slurry were dispersed in water for measurement. Each curve is an average of 3 measurements.

IV. Characterisation of MOF Composite Films

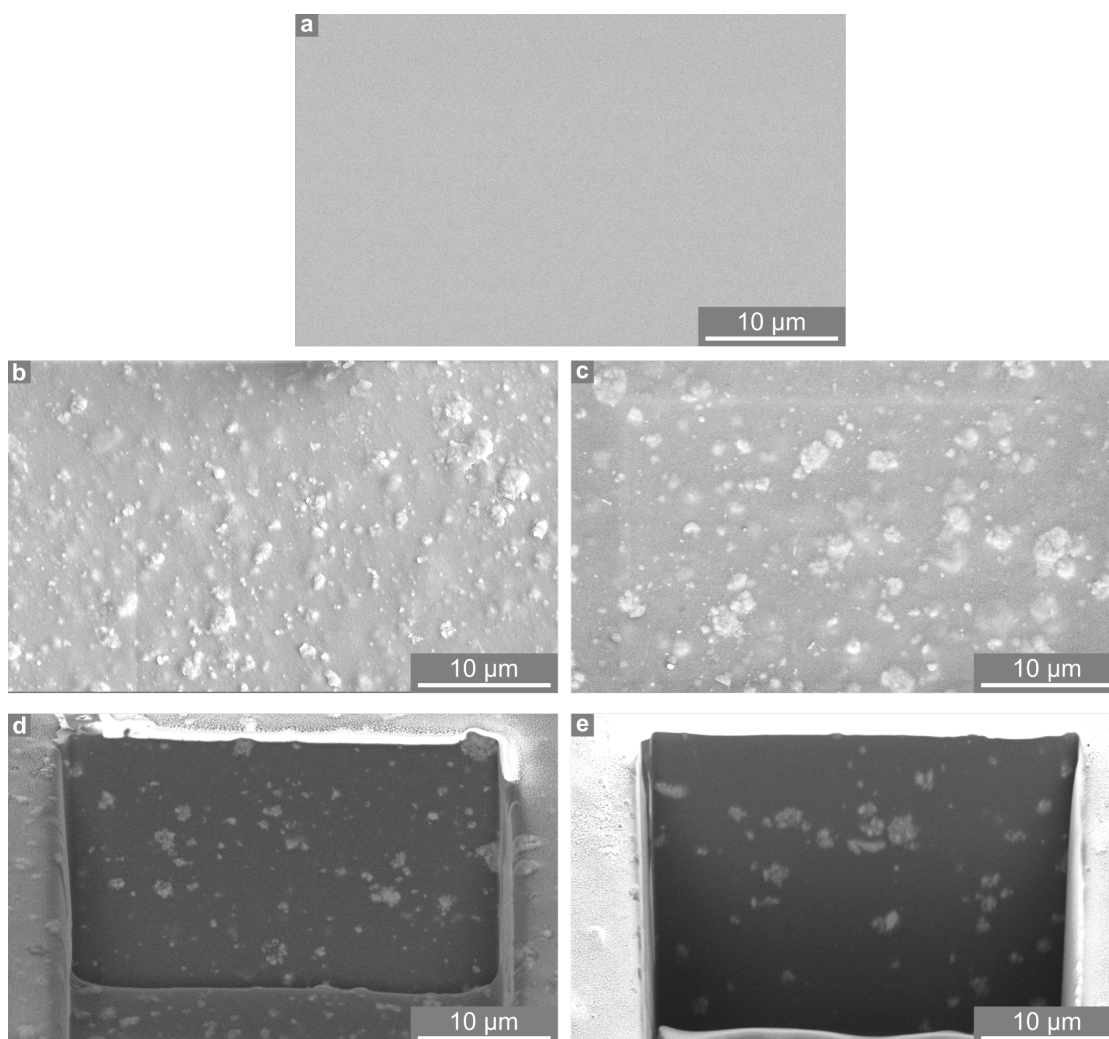


Figure S4. SEM micrographs a) surface of blank polyurethane film, b) surface of **CPO-27-Ni-HT** – 5 wt% MOF, c) surface of **CPO-27-Ni-RT** – 5 wt% MOF, d) cross sectional area of **CPO-27-Ni-HT** – 5 wt% MOF and e) cross sectional area of **CPO-27-Ni-RT** – 5 wt% MOF composite films.

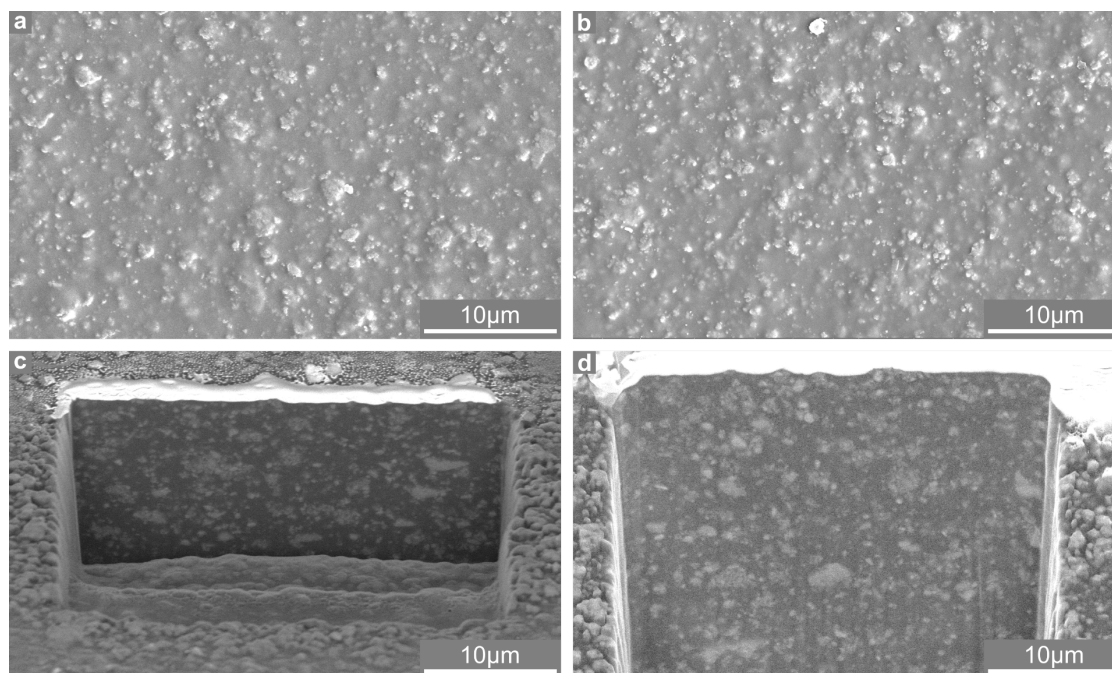


Figure S5. SEM micrographs a) surface of **CPO-27-Ni-HT** - 20 wt% MOF, b) surface of **CPO-27-Ni-RT** - 20 wt% MOF, c) cross sectional area of **CPO-27-Ni-HT** - 20 wt% MOF and d) cross sectional area of **CPO-27-Ni-RT** - 20 wt% MOF composite films.

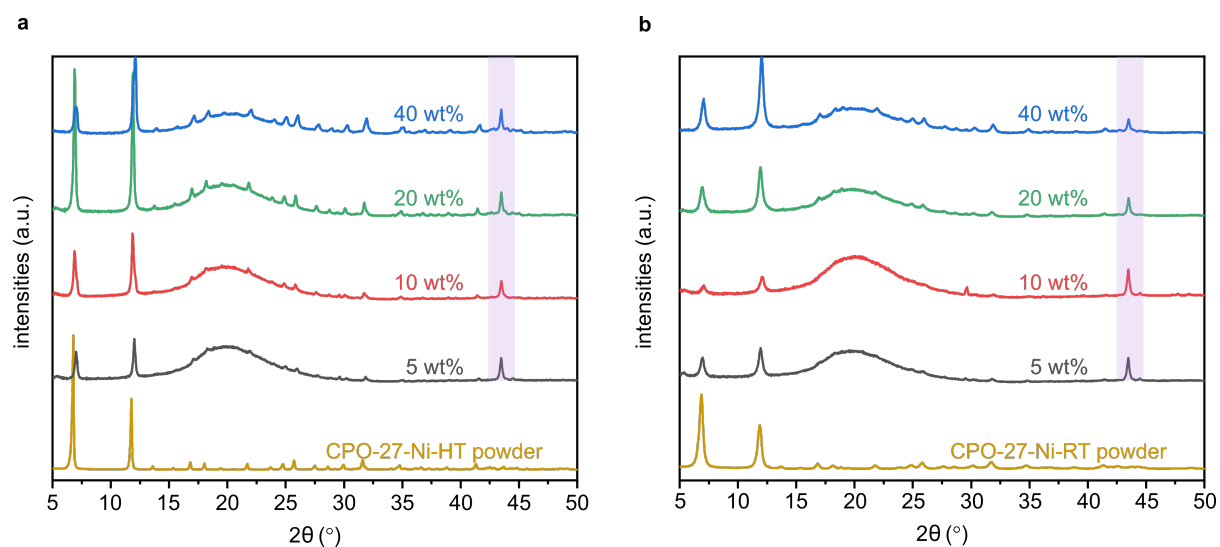


Figure S6. PXRD patterns of MOF composite films and respective MOF powder. a) **CPO-27-Ni-HT** powder (mustard), **CPO-27-Ni-HT** - 5 wt% (gray), **CPO-27-Ni-HT** - 10 wt% (red), **CPO-27-Ni-HT** - 20 wt% (green), and **CPO-27-Ni-HT** - 40 wt% (blue) and b) **CPO-27-Ni-RT** (mustard), **CPO-27-Ni-RT** - 5 wt% (gray), **CPO-27-Ni-RT** - 10 wt% (red), **CPO-27-Ni-RT** - 20 wt% (green), and **CPO-27-Ni-RT** - 40 wt% (blue). Reflection highlighted (purple shading) attributable to steel sample holder.

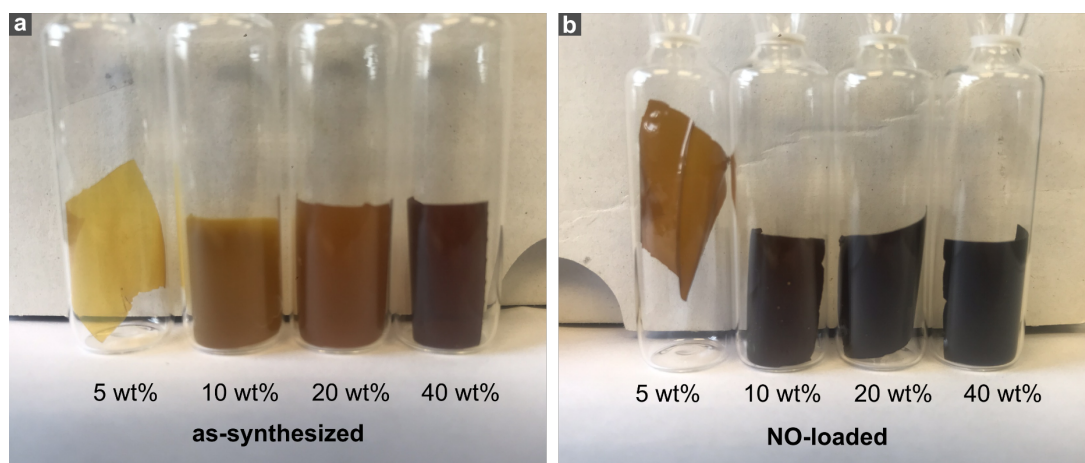


Figure S7. Photographs of **CPO-27-Ni-HT** composite films containing 5, 10, 20 and 40 wt% MOF loading levels. a) As synthesized films and b) after activation and NO loading, vials are sealed under Ar.

V. NO Release Performance of MOF Powders and Composite Films

Table S3. Tabulation of the total number of mmoles of NO released as per quantity of film and MOF, and duration of release for both powder **CPO-27-Ni** (HT and RT) materials and composite films containing **CPO-27-Ni** (HT and RT) at 5, 10, 20 and 40 wt% MOF loading levels. Data acquisition stopped when concentration of NO released reached 30ppb.

MOF loading (wt%)	CPO-27-Ni-HT			CPO-27-Ni-RT		
	Total NO released (mmol/g film)	Total NO released (mmol/g MOF)	Duration of release (h)	Total NO released (mmol/g film)	Total NO released (mmol/g MOF)	Duration of release (h)
Powder	/	6.22	32	/	3.50	25
5 wt%	0.08 ± 0.001	1.56 ± 0.03	22	0.05 ± 0.046	0.97 ± 0.092	10
10 wt%	0.19 ± 0.003	1.92 ± 0.03	40	0.12 ± 0.008	1.20 ± 0.084	15
20 wt%	0.25 ± 0.002	1.25 ± 0.01	45	0.19 ± 0.007	0.92 ± 0.036	45
40 wt%	0.20 ± 0.016	0.52 ± 0.04	66	0.18 ± 0.011	0.49 ± 0.028	92

VI. Water Adsorption Isotherm Data

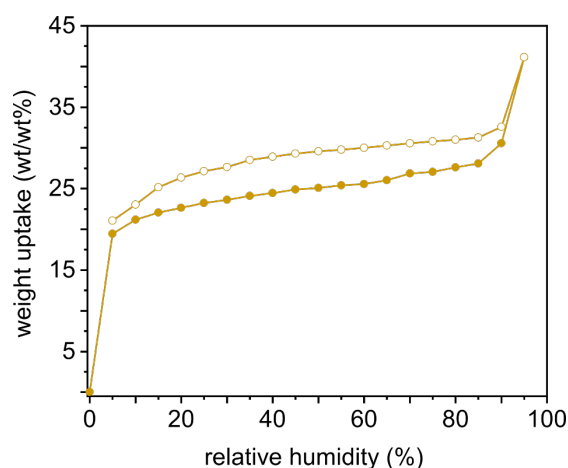


Figure S8. Water adsorption isotherm for powder **CPO-27-Ni-RT** material. Closed symbols refer to adsorption and open symbols to desorption.

Table S4. Water adsorption isotherm data for blank polymer film, **CPO-27-Ni-RT** composite films containing 5, 10, 20 and 40 wt% MOF loading levels and powder **CPO-27-Ni-RT** material.#

Material	Maximum Water Uptake at 95% RH (wt/wt%)	Duration of Experiment (h)	Hysteresis at 25% RH (wt/wt%)	Hysteresis at 50% RH (wt/wt%)
blank polymer film	1.12	23.5	0.02	0.07
5 wt% CPO-27-Ni-RT film	2.67	47.0	0.34	0.42
10 wt% CPO-27-Ni-RT film	3.77	63.5	0.61	0.58
20 wt% CPO-27-Ni-RT film	5.97	84.0	1.09	1.18
40 wt% CPO-27-Ni-RT film	9.05	151.0	1.97	2.28
CPO-27-Ni-RT powder	41.15	264.0	3.87	4.47

#(note the accuracy of the balance is 1 μ g, therefore although the range of values is small, it is believed to be within the accuracy of the measurement).

VII. Antibacterial Testing

Table S5. Tabulation of the cell densities and standard error values from the antibacterial testing results of **CPO-27-Ni-RT -10 wt% MOF as prepared film** and **CPO-27-Ni-RT -10 wt% MOF NO loaded film** against Gram negative bacteria *P. aeruginosa* ATCC 15442 following incubation times of 5 h and 24 h. The standard error of the mean is for N=6. The control was a blank polyurethane film.

Sample	After 5 h Incubation		After 24 h Incubation	
	Cell Density (CFU/mL)	Standard Error (CFU/mL)	Cell Density (CFU/mL)	Standard Error (CFU/mL)
<i>P. aeruginosa</i>	4.23×10^6	4.67×10^5	1.57×10^8	5.84×10^6
blank polymer film	9.17×10^6	2.74×10^6	8.00×10^8	7.21×10^7
10 wt% CPO-27-Ni-RT film as prepared	1.03×10^7	3.38×10^6	5.23×10^8	4.91×10^7
10 wt% CPO-27-Ni-RT film loaded with NO	6.57×10^3	2.76×10^3	no growth	-

VIII. Computational Methods

DFT Calculations:

In these calculations both the positions of the atoms of the framework and the unit cell parameters for the bulk structure were fully relaxed. The PBE functional¹ was used along with a combined Gaussian basis set and plane wave pseudopotential strategy as implemented in the code. A triple zeta Gaussian-type basis set (TZVP-MOLOPT basis set provided with the code)² was considered for all atoms, except for the metal centers, where double zeta functions were employed (DZVP-MOLOPT).³ The pseudopotentials used for all of the atoms were those derived by Goedecker, Teter and Hutter.^{3,4} These calculations included the semi-empirical dispersion corrections as implemented in the DFT-D3 method, derived by Grimme.⁴ From the resulting optimized structure, a set of Miller indices that would result in a favorable surface cut was identified via the Bravais-Friedel-Donnay-Harker (BFDH) method.^{5,6} The {101} surface slab model was then constructed. As in our previous work, the surface was reconstructed so as to assure dipole neutrality along the z-axis. The final slab consisted of 10 “layers”, as defined by the inter-layer d-spacing. The strategy for capping the under-coordinated metal sites involved coordination of free water molecules to these atoms. The final model was then geometry-optimized using the Quickstep module of the CP2K code,⁷ using the same level of theory and

parameters as for the optimization of the bulk model. Here the cell parameters were held fixed, as were the atoms corresponding to the inner 6 layers. The charges for the material were taken from our previous study.⁸

Equilibration of MOF/Polymer Interfaces:

Force field-based MD simulations were run to equilibrate the polymer in the direction perpendicular to the MOF surface. Seven cycles of three simulations were performed, out of which the first two were carried out in the canonical ensemble at $T=600$ K and $T=300$ K respectively, and the last one in the NP_nT ensemble with $T=300$ K and P_n the pressure normal to the MOF surface (z direction). The pressure was set up to $P_n = 0.2, 6, 10, 5, 1, 0.1$ or 0.001 kbar, for each of the seven cycles. The values for temperature and pressure were obtained by applying this same protocol to the equilibration of the pure polymer, which had yielded a reasonable density, compared to experiment. Berendsen thermostat and barostat⁹ (the latter one modified to apply the pressure only in the direction normal to the MOF surface) were used, with relaxation times of 0.1 and 0.5 ps respectively. A modified version of DLPOLY classic was used for the interface generation and production simulations.¹⁰

This procedure was used and validated by comparing with Biased Potential Dynamics results in our previous work, where the methodology for building MOF/polymer interfaces was first developed.¹¹

Polyurethane Force Field:

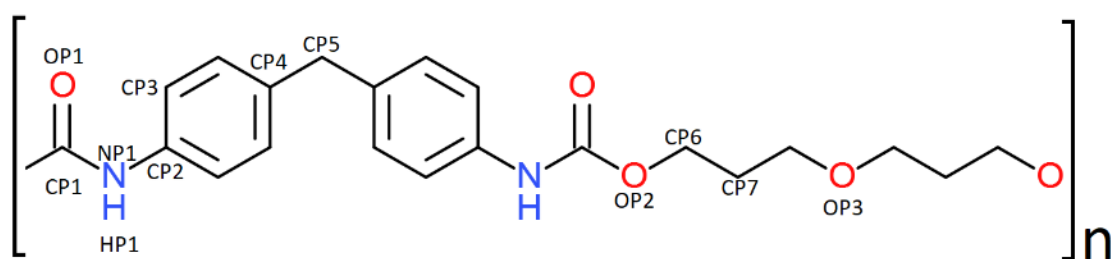


Figure S9. Scheme of the monomer of the modelled polyurethane, including force field atom types.

Table S6. Non bonded force field parameters for polyurethane. 12-6 LJ parameters were extracted from TraPPE-UA, charges were computed in this work as detailed in the manuscript

Atom Type	$\sigma_{ii}(\text{\AA})$	$\epsilon_{ii}(\text{kcal/mol})$	q_i (e)
OP1	3.050	0.15700	-0.600
CP1	3.820	0.07950	0.996

NP1	3.340	0.22060	-0.831
HP1	0.500	0.00238	0.388
CP2	3.850	0.03970	0.444
CP3	3.695	0.10040	-0.082
CP4	3.850	0.03970	0.218
CP5	3.950	0.09140	-0.112
OP2	2.800	0.10900	-0.491
CP6	3.950	0.09140	0.184
CP7	3.950	0.09140	0.095
OP3	2.800	0.10900	-0.406

Table S7. Bond force field parameters for polyurethane. Parameters were extracted from GAFF, for the following equation:
 $E_{bond} = k(d-d_0)^2$.

Bond	k(kcal/mol Å ²)	d ₀ (Å)
OP1-CP1	648.0	1.214
CP1-NP1	478.2	1.345
NP1-HP1	410.2	1.009
NP1-CP2	372.3	1.422
CP2-CP3	478.4	1.387
CP3-CP3	478.4	1.387
CP3-CP4	478.4	1.387
CP4-CP5	478.4	1.387
CP1-OP2	411.3	1.343
OP2-CP6	301.5	1.439
CP6-CP7	303.1	1.535
CP6-OP3	301.5	1.439

OP2-HP1	369.6	0.974
---------	-------	-------

Table S8. Angle force field parameters for polyurethane. Parameters were extracted from GAFF for the following equation: $E_{angle} = k(\theta - \theta_0)^2$.

Angle	k(kcal/mol rad ²)	θ_0 (deg)
OP1-CP1-NP1	75.83	122.03
CP1-NP1-HP1	49.21	118.46
CP1-NP1-CP2	64.29	123.71
HP1-NP1-CP2	47.36	115.94
NP1-CP2-CP3	67.97	119.89
CP3-CP2-CP3	67.18	119.97
CP2-CP3-CP3	67.18	119.97
CP3-CP3-CP4	67.18	119.97
CP3-CP4-CP3	67.18	119.97
CP3-CP4-CP5	63.84	120.63
CP4-CP5-CP4	63.66	112.26
NP1-CP1-OP2	76.68	109.28
OP2-CP1-OP1	75.93	123.33
CP1-OP2-CP6	63.63	115.14
OP2-CP6-CP7	67.78	108.42
CP6-CP7-CP6	63.21	110.63
CP7-CP6-OP3	67.78	108.42
CP6-OP3-CP6	62.39	112.45

Table S9. Dihedral angle force field parameters for polyurethane. Parameters were extracted from GAFF for the following equation: $E_{dihedral} = k[1 + d\cos(n\phi)]$.

Dihedral	k(kcal/mol)	D	N
----------	-------------	---	---

OP1-CP1-NP1-HP1	5.000	-1	2
OP1-CP1-NP1-CP2	5.000	-1	2
CP1-NP1-CP2-CP3	0.900	-1	2
HP1-NP1-CP2-CP3	0.900	-1	2
NP1-CP2-CP3-CP3	7.250	-1	2
CP3-CP2-CP3-CP3	7.250	-1	2
CP2-CP3-CP3-CP4	7.250	-1	2
CP3-CP3-CP4-CP3	7.250	-1	2
CP3-CP3-CP4-CP5	7.250	-1	2
CP3-CP4-CP5-CP4	0.000	1	2
CP2-NP1-CP1-OP2	5.000	-1	2
HP1-NP1-CP1-OP2	5.000	-1	2
NP1-CP1-OP2-CP6	0.900	-1	2
OP1-CP1-OP2-CP6	2.700	-1	2
CP1-OP2-CP6-CP7	0.575	1	3
OP2-CP6-CP7-CP6	0.700	1	3
CP6-CP7-CP6-OP3	0.700	1	3
CP7-CP6-OP3-CP6	0.750	1	3

CPO-27-Ni surface Force Field:

Table S10. Force field parameters for CPO-27-Ni. 12-6 LJ parameters were extracted from (*) UFF, (**) DREIDING, charges were computed in this work as detailed in the manuscript.

Atom Type	$\sigma_{ii}(\text{\AA})$	$\epsilon_{ii}(\text{kcal/mol})$	$q_i (e)$
Ni*	2.525	0.0150	1.884990
Nis*	2.525	0.0150	1.895280
ow*	3.118	0.0600	-1.027000

ows*	3.118	0.0600	-1.044500
O2**	3.033	0.0957	-1.043540
O3**	3.033	0.0957	-1.042480
Os**	3.033	0.0957	-1.043000
C1**	3.473	0.0951	1.041000
C2**	3.473	0.0951	-0.222000
C3**	3.473	0.0951	0.566000
C4**	3.473	0.0951	-0.296000
H1**	2.846	0.0152	0.300000
hw*	2.571	0.0440	0.450000
hws*	2.571	0.0440	0.464129

Note: The charges are cited to 6 decimal places, as this allows one to obtain a neutral cell when passing from a cluster to a periodic model.

IX. References

- (1) Perdew, J. P.; Burke, K.; Ernzerhof, M. Generalized Gradient Approximation Made Simple. *Phys. Rev. Lett.* **1996**, *77* (18), 3865–3868. <https://doi.org/10.1103/PhysRevLett.77.3865>.
- (2) VandeVondele, J.; Hutter, J. Gaussian Basis Sets for Accurate Calculations on Molecular Systems in Gas and Condensed Phases. *J. Chem. Phys.* **2007**, *127* (11), 114105. <https://doi.org/10.1063/1.2770708>.
- (3) Goedecker, S.; Teter, M.; Hutter, J. Separable Dual-Space Gaussian Pseudopotentials. *Phys. Rev. B* **1996**, *54* (3), 1703–1710. <https://doi.org/10.1103/PhysRevB.54.1703>.
- (4) Grimme, S. Semiempirical GGA-Type Density Functional Constructed with a Long-Range Dispersion Correction. *J. Comput. Chem.* **2006**, *27* (15), 1787–1799. <https://doi.org/10.1002/jcc.20495>.
- (5) Donnay, J. D. H.; Harker, D. A New Law of Crystal Morphology Extending the Law of Bravais. *Am. Miner.* **1937**, *22*, 446.
- (6) Friedel, G. Études Sur La Loi de Bravais. *Bull. la Société française Minéralogie* **1907**, *30* (9), 326–455. <https://doi.org/10.3406/bulmi.1907.2820>.
- (7) Hutter, J.; Iannuzzi, M.; Schiffmann, F.; VandeVondele, J. Cp2k: Atomistic Simulations of Condensed Matter Systems. *Wiley Interdiscip. Rev. Comput. Mol. Sci.* **2014**, *4* (1), 15–25.

<https://doi.org/10.1002/wcms.1159>.

- (8) Zheng, J.; Barpaga, D.; Trump, B. A.; Shetty, M.; Fan, Y.; Bhattacharya, P.; Jenks, J. J.; Su, C.-Y.; Brown, C. M.; Maurin, G.; McGrail, B. P.; Motkuri, R. K. Molecular Insight into Fluorocarbon Adsorption in Pore Expanded Metal–Organic Framework Analogs. *J. Am. Chem. Soc.* **2020**, *142* (6), 3002–3012. <https://doi.org/10.1021/jacs.9b11963>.
- (9) Berendsen, H. J. C.; Postma, J. P. M.; van Gunsteren, W. F.; DiNola, A.; Haak, J. R. Molecular Dynamics with Coupling to an External Bath. *J. Chem. Phys.* **1984**, *81* (8), 3684–3690. <https://doi.org/10.1063/1.448118>.
- (10) Todorov, I. T.; Smith, W.; Trachenko, K.; Dove, M. T. DL_POLY_3: New Dimensions in Molecular Dynamics Simulations via Massive Parallelism. *J. Mater. Chem.* **2006**, *16* (20), 1911. <https://doi.org/10.1039/b517931a>.
- (11) Semino, R.; Ramsahye, N. A.; Ghoufi, A.; Maurin, G. Microscopic Model of the Metal–Organic Framework/Polymer Interface: A First Step toward Understanding the Compatibility in Mixed Matrix Membranes. *ACS Appl. Mater. Interfaces* **2016**, *8* (1), 809–819. <https://doi.org/10.1021/acsami.5b10150>.